Pergamon

Chaos, Solitons & Fractals, Vol. 8, No. 3, pp. 313–326, 1997

0960-0779/97 $17.00 + 0.00

PII: S0960-0779(96)00131-2

Feedback Control of Chaotic Circular Point Sets with Arbitrary Velocity Profile

Z. YONG and R. KOVACEVIC

Center for Robotics and Manufacturing Systems, University of Kentucky, Lexington, KY 40506-0108, USA

(Accepted 31 October 1996)

Abstract—To simulate general particle motion on the cross-section of a particle laden jetflow by using fractal point sets, a feedback control process is developed to ensure the validity of nonlinear mapping techniques that transform an original fractal point set into the point set with any desired velocity profile. The points are utilized to represent quantitatively functional abrasive particles in abrasive waterjets which are capable of penetrating hard-to-machine materials such as titanium and advanced ceramics. The theoretical framework constitutes one of the most important parts in three-dimensional modeling of particle jetflow machining. Experimental results from cutting titanium and aluminum verify that the model has very good accuracy. © 1997 Elsevier Science Ltd

1. INTRODUCTION

In a previous investigation [1], it was proven that a fractal point set with chaotic and axisymmetrical features can be used to simulate the particle motion on a cross-section of a particle laden jetflow. This can be used in evaluating the erosion rate of high speed particles impacting a workpiece, as shown in Fig. 1. A crucial step of this approach is the mapping of an original point set to another one which has any desired velocity profile and geometrical configuration.

Because of the nonlinearity carried with mapping, an interesting issue naturally arises: How can one find a suitable point set to fit the physical conditions from non-unique mapping results? For example, mapping the axisymmetrical point set $f_p = \{(r_1, \vartheta_1),(r_2, \vartheta_2),\ldots,(r_n, \vartheta_n)\}$ to another point set $f_p^M = \{(\zeta_1, \vartheta_1),(\zeta_2, \vartheta_2),\ldots,(\zeta_n, \vartheta_n)\}$ with the velocity profile of laminar flow, the equation (see Ref. [1]) is of the form

$$\zeta_k^2(2 - \zeta_k^2) = 1 - (1 - r_k)^{11/10}(1 + \tfrac{11}{10}r_k), \quad k = 1,2,\ldots,n. \tag{1}$$

Obviously, eqn (1) has four solutions. After careful analysis, the correct mapping equation is given by

$$\zeta_k = [1 - ((1 - r_k)^{11/10}(1 + \tfrac{11}{10}r_k))^{1/2}]^{1/2} \tag{2}$$

and the other three solutions to eqn (1) are trivial ones. One should bear in mind that this is possibly the simplest mapping equation involved in the subject. Usually, an explicit mapping expression is not available for a general case. Therefore, the search for new point sets becomes intrinsically difficult because of the existence of non-unique solutions. In order to eliminate the uncertainty of mapping results, a feedback control process is developed through adjusting the various variables relevant to nonlinear transformations. The validity of this approach will be justified by both analytical and experimental demonstrations. Concerning research activities of other topics in the control of chaos, readers are invited to scan the recent reviews [2, 3].

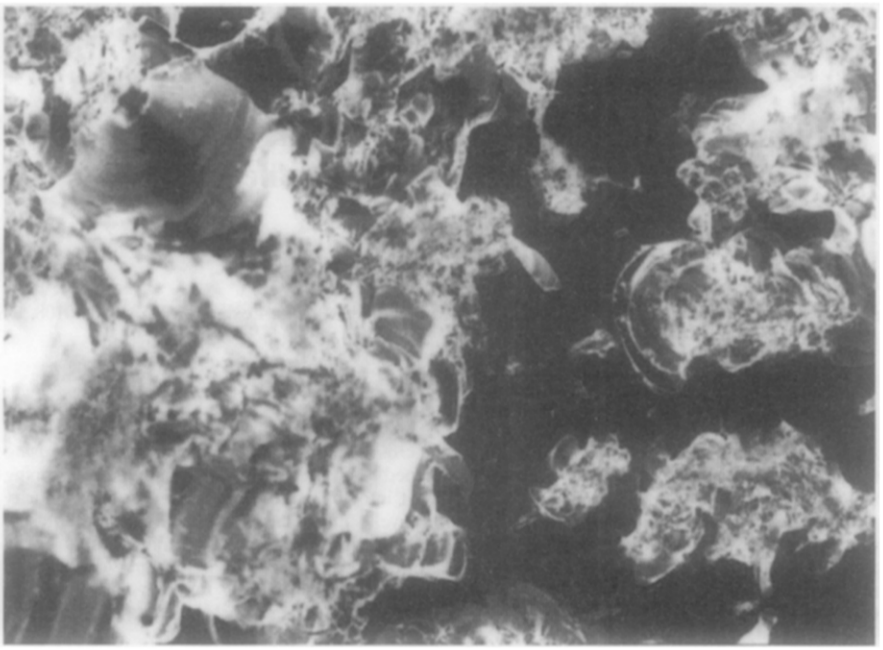

Fig. 1. Micro craters ($\times 200$) created by particle impact on the glass plate.

In this research, attention is focused on the axisymmetrical particle jetflow because of its wide applications and moderate mathematical involvement. In this circumstance, the angle mapping is not necessary. This work is oriented toward the simulation of abrasive waterjet (AWJ) machining, which involves the interaction between a workpiece and three-phase jetflow (abrasives, water and air). In the sequel, macro and micro machining parameters are used to verify the analytical results.

2. ORIGINAL POINT SET

A point set generated from iterative equations will be analyzed in detail to verify its capacity of representing, geometrically and physically, a particle source. In the light of the conditions of particle motion on a circular cross-section, the point set should possess two general features. Specifically, the appearance of particles is disordered or chaotic and the global distribution of particles is approximately axisymmetrical after the number of particles passing through the cross-section exceeds a certain value. Under the Cartesian and polar coordinate systems (x,y) and (r,θ), computational experimentation shows that these criteria are satisfied by the set f_p, where

$$f_p = \{(x_1,y_1),(x_2,y_2),\ldots,(x_n,y_n)\} = \{(r_1,\theta_1),(r_2,\theta_2),\ldots,(r_n,\theta_n)\} \subset J, \tag{3}$$

$$0 \le r_n = \sqrt{x^2{}_n + y^2{}_n} \le 1, \tag{4}$$

$$0 \le \theta_n = \arctan(y_n/x_n) < 2\pi, \quad n = 0,1,2,\ldots, \tag{5}$$

where $J = \{(\xi_1,\eta_1),(\xi_2,\eta_2),\ldots,(\xi_N,\eta_N)\}$ is a Julia set (fractal point set) produced by the iterative equations

$$\xi_{N+1} = [(R(\xi_N,\eta_N))^2 + (I(\xi_N,\eta_N))^2]^{1/4}\cos(\theta(\xi_N,\eta_N)/2) - 0.368, \tag{6}$$

$$\eta_{N+1} = [(R(\xi_N,\eta_N))^2 + (I(\xi_N,\eta_N))^2]^{1/4}\sin(\theta(\xi_N,\eta_N)/2) + 0.4436, \tag{7}$$

with

$$R(\xi_N, \eta_N) = \xi_N^3 - 3\xi_N\eta_N^2 + 1.24(\eta_N^2 - \xi_N^2), \tag{8}$$

$$I(\xi_N, \eta_N) = -\eta_N^3 + 3\eta_N\xi_N^2 - 2.48\eta_N\xi_N, \tag{9}$$

$$-\pi < \theta(\xi_N, \eta_N) = \arctan\left(\frac{I(\xi_N, \eta_N)}{R(\xi_N, \eta_N)}\right) \le \pi, \tag{10}$$

$$x_n = 5\xi_N + 0.70, \quad y_n = 5\eta_N - 1.5. \tag{11}$$

A very brief description was given in [1] about the complex form of the iterative eqns (6) and (7). Next, the two features of f_p stated above will be demonstrated.

2.1. *Chaotic feature*

Many alternative mathematical techniques are available to display the unpredictable appearance of points $(x_n, y_n) \in f_p$ on a circular domain $0 \le r_n \le 1$ with respect to iterative order n. Here the spectrum patterns of x_n vs n and y_n vs n are chosen to visualize the fact. Two examples are shown in Fig. 2. Particles are non-periodically scattered over the plane domain and a position distribution of this kind is sensitive to the constants of iteration equations. Although the number of points displayed in each pattern is limited, it is easy to obtain more patterns, like these with arbitrary intervals of n. It is necessary to indicate that the iterative process may blow out when the constants in eqns (6) and (7) or the initial values ξ_0 and η_0 are slightly changed.

2.2. *Axisymmetrical feature*

In terms of the geometrical constraints on particles in a jetflow, it is expected that the distribution of particles on the circular cross-section should be axisymmetrical after the number of particles passing through the section is greater than a certain value. To measure this feature, four akin parameters are introduced as the criterion

$$\gamma_1 = p_1(\theta_n)/\bar{p}, \quad \gamma_2 = p_2(\theta_n)/\bar{p}, \quad \gamma_3 = p_3(\theta_n)/\bar{p}, \quad \gamma_4 = p_4(\theta_n)/\bar{p}, \tag{12}$$

where $p_i(\theta_n)$, $i = 1,2,3,4$, are the particle numbers for any given n in the four domains

$$s_1: 0 \le \theta < \pi/2, \quad s_2: \pi/2 \le \theta < \pi, \quad s_3: \pi \le \theta < 3\pi/2, \quad s_4: 3\pi/2 \le \theta < 2\pi. \tag{13}$$

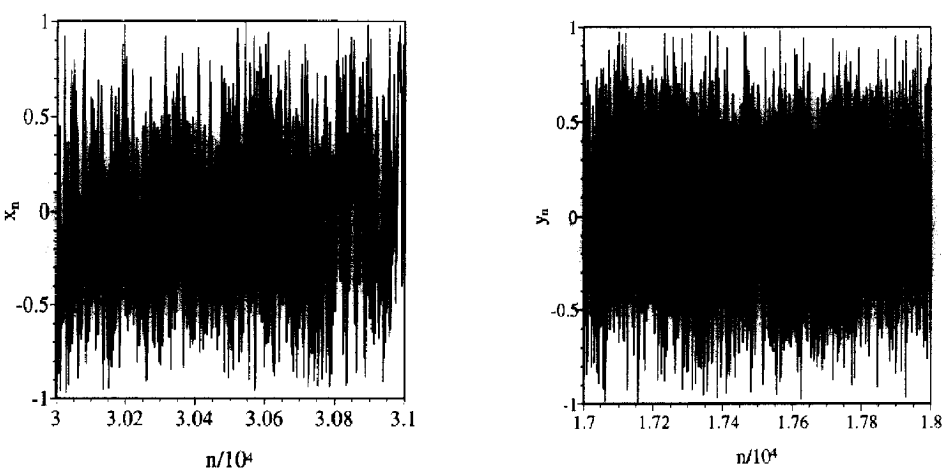

Fig. 2. Demonstration of chaotic appearance of point set f_p.

and $\bar{p} = (p_1 + p_2 + p_3 + p_4)/4 = n/4$ is the average number of each domain. For an ideal axisymmetrical point set, one can easily conclude that $\gamma_1 = \gamma_2 = \gamma_3 = \gamma_4 = 1$ holds for any rotary transformation on f_p. To check the potential error of f_p, a rotation mapping

$$T(\alpha) = e^{\alpha i}, \quad 0 \le \alpha < 2\pi, \tag{14}$$

is applied to each point of the subdomain s_i, for $i = 1,2,3,4$. As a result, the positions of all the particles vary with the rotation angle α and hence γ_i, $i = 1,2,3,4$, are converted to

$$\gamma_1(\alpha) = p_1(\theta_n + \alpha)/\bar{p}, \quad \gamma_2 = p_2(\theta_n + \alpha)/\bar{p}, \quad \gamma_3 = p_3(\theta_n + \alpha)/\bar{p}, \quad \gamma_4 = p_4(\theta_n + \alpha)/\bar{p}, \tag{15}$$

since

$$z_n T(\alpha) = r_n e^{\theta_n i} e^{\alpha i} = r_n e^{(\theta_n + \alpha)i}, \tag{16}$$

where

$$z_n = x_n + iy_n = r_n e^{i\theta_n}. \tag{17}$$

The geometric meaning of eqn (15) is that when α varies from 0 to 2π, particles of each domain experience a periodic relocation. Therefore, if the values of $\gamma_i(\alpha)$ are only very weakly dependent on α for any given n, then f_p is said to satisfy the axisymmetrical condition. As shown in Fig. 3, after n exceeds 5×10^3, the non-axisymmetric error calculated by $\gamma_i(\alpha) - \alpha$ is consistently less than 8%. This means that f_p has a good axisymmetric characteristic.

It turns out that point set f_p can be used to describe the motion of particles on the circular cross-section of steady axisymmetric particle laden flow. Most importantly, the position of every particle is quantitatively ascertained by the coordinates of a corresponding point, and therefore the traces of a particle can be accurately followed even when the jetflow moves with the nozzle. Since the machining of solid materials by abrasive waterjet is the erosion result of millions of individual particles, the finding of f_p enables researchers or engineers to build a three-dimensional model for predicting the penetration ability of particles.

3. VELOCITY PROFILE OF f_p

Do the points of f_p possess velocities along the direction of flow in a nozzle? The answer is firmly positive if the points are identified by particles of jetflow through a physical principle.

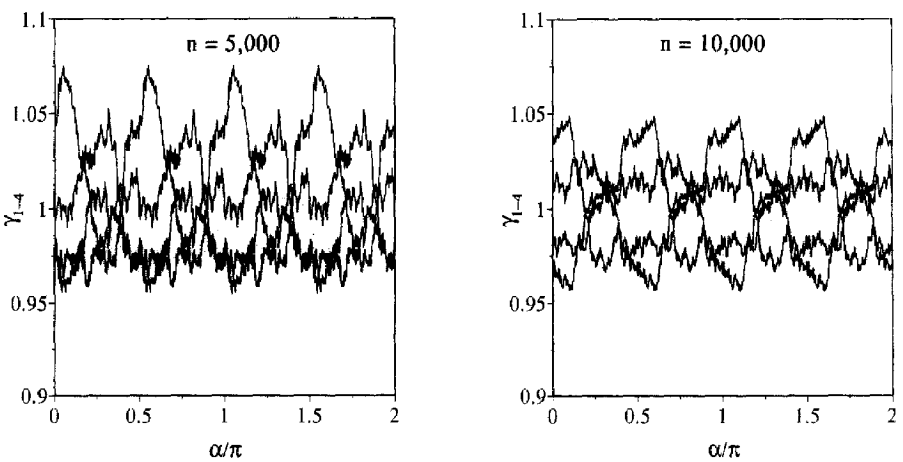

Fig. 3. Demonstration of axisymmetrical features of particle distribution.

After being endowed with a velocity profile, a point set is said to be a functional one since it contains kinetic energy.

To visualize the velocity profile of f_p, two assumptions for particle motion in three-phase laden flow are introduced into this analysis: (a) that the velocity profile of the particles is equal or similar to the average velocity profile of three-phase flow, and (b) that the mixture of particles, water and air is uniform, which means that the density of particles is a constant. A proof for the second assumption was given in [1]. Subject to these two constraints, application of the mass conservation principle to the local volume flowrate leads to an important ratio

$$R_f = \frac{N_{xy}}{N_0} = \frac{1}{k_0}\left[\int_{x_0}^{x} \mathrm{d}\xi \int_{y_0}^{y} V_z(t,\xi,\eta)\,\mathrm{d}\eta\right]\left[\int_{S_0} V_z(t,\xi,\eta)\,\mathrm{d}\xi\,\mathrm{d}\eta\right]^{-1}, \tag{18}$$

satisfying $0 \le R_f \le 1$, where S_0 is the area of a cross-section, which is not necessarily circular, and $S_{xy} = (x - x_0)(y - y_0)$ is a subdomain of S_0, V_z is the average velocity of three-phase flow, N_{xy} is the number of particles passing through S_{xy} at the instant t, N_0 is the number of particles passing through S_0, and k_0 is a constant. The physical meaning of R_f is the ratio of local volume flowrate to the entire volume flowrate. For brevity R_f is hereinafter called the flowrate ratio.

For steady axisymmetric annular flow, eqn (18) reduces to

$$R_f = \frac{N_{xy}}{N_0} = \frac{1}{k_0}\left[\int_{\rho}^{r} V_z(r) r\,\mathrm{d}r\right]\left[\int_{\rho}^{1} V_z(r) r\,\mathrm{d}r\right]^{-1}, \quad \rho \le r \le 1, \tag{19}$$

where ρ is the ratio of the interior radius to the exterior radius of the pipe. It is easy to see that the average velocity V_z can be expressed by the derivative of R_f as

$$V_z = k_0\left[\int_{\rho}^{1} V_z(r) r\,\mathrm{d}r\right]\frac{1}{r}\frac{\mathrm{d}R_f}{\mathrm{d}r}. \tag{20}$$

After normalization, eqn (20) can be rewritten as

$$V_{zp} = \frac{V_z}{(V_z)_{\max}} = \left(\frac{1\mathrm{d}R_f}{r\,\mathrm{d}r}\right)\left(\frac{1\mathrm{d}R_f}{r\,\mathrm{d}r}\right)^{-1}_{\max}, \quad 0 \le V_{zp} \le 1. \tag{21}$$

In general, $R_f = N_{xy}/N_0$ is a discrete function relevant to instant particle numbers and thus the value of $\mathrm{d}R_f/\mathrm{d}r$ can be determined only by numerical differentiation

$$\frac{\mathrm{d}R_f}{\mathrm{d}r} = \frac{R_f(r_i) - R_f(r_{i-1})}{r_i - r_{i-1}}, \quad i = 1,2,.... \tag{22}$$

The initial value r_0 and increment $\Delta r = r_i - r_{i-1}$ of radius have significant influences on the accuracy of $\mathrm{d}R_f/\mathrm{d}r$. Based on eqns (19), (20) and (21), the velocity V_{zp} and the volume flowrate ratio R_f of f_p are ascertained. In addition, computations show that the analytical functions

$$\bar{V}_{zp}(r) = (1 - r)^{1/10}, \tag{23}$$

$$\bar{R}_f = 1 - (1 - r)^{11/10}(1 + \tfrac{11}{10}r), \tag{24}$$

can be used [1] to represent accurately the average values of V_{zp} and R_f for f_p.

4. CONTROL OF VELOCITY PROFILE

During the machining of a mechanical part, the velocity profile of an abrasive waterjet could change dramatically. For instance, the jetflow may vary from turbulent flow to laminar

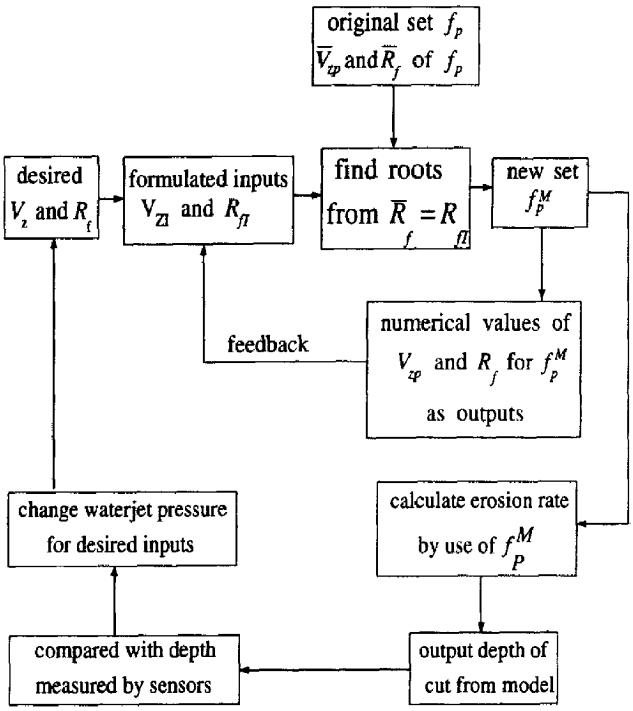

Fig. 4. Diagram of control process for generating new desired point sets.

flow. This issue arises because diverse particle velocities are needed for cutting different materials or performing distinct functions. As described previously, the uncertainty of results appears because of the nonlinearity of mappings. Therefore, in order to simulate a machining process, a robust control process must be designed to convert V_{zp} and R_f of f_p to any desired ones which match practical requirements. In other words, a new point set f_p^M, apart from f_p, will be formed as the output of a control system, for any desired local flowrate ratio and velocity profile. The control process is illustrated in Fig. 4 and the function of each element is explained in detail below.

4.1. *Analytical representation of input velocity V_{zl}*

In a general case, the average velocity profile of multiphase flow can be described only in the form of discrete data resulting from either experimental measurements or numerical calculations, especially for turbulent flow. Suppose that a group of known data with L numbers is the numerical representation of the velocity profile for an annular flow, expressed by matrix $\mathbf{C}^{\mathrm{T}} = [c_1, c_2, \ldots, c_L]$. For the convenience of analysis, a polynomial equation is adopted to express approximately the normalized velocity, i.e.

$$V_{zl} = \sum_{i=1}^{L} b_i r^{i-1}, \quad \rho \le r \le 1, 0 \le V_{zl} \le 1, \tag{25}$$

where $\rho = r_{\mathrm{I}}/r_{\mathrm{E}}$ is the ratio of interior radius r_{I} to exterior radius r_{E} of the annular flow. The coefficient matrix $\mathbf{B}^{\mathrm{T}} = [b_1, b_2, \ldots, b_L]$ for eqn (25) is determined by the equation

$$\mathbf{BA} = \mathbf{C}, \tag{26}$$

where the general element a_{ij} of matrix $\mathbf{A}$ is given by $a_{ij} = r_i^{j-1}$, for $i,j = 1,2,..,L$. Clearly the

accuracy of eqn (26) is related to the number L of polynomial terms. Nevertheless, the increase of L does not necessarily mean an improvement of control accuracy, especially for turbulent flow because its average velocity profile changes sharply near the boundaries.

If the velocity profile of the three-phase jetflow is assumed to be similar to that of one-phase axisymmetric laminar flow, based on the classical result [4], its dimensionless expression is written as the normalized form

$$V_{zl} = \frac{1}{V_{\max}}\left[1 - r^2 + \frac{\ln r}{\ln \rho}(V_\rho - 1 + \rho^2)\right], \quad \rho \le r \le 1, \tag{27}$$

where $V_\rho = v_\rho / k$ (k being a physical constant) is the dimensionless velocity of flow at $r = \rho$, which may not be zero since the flow contacts with non-stationary boundary, and $V_{\max}$ is the maximum value of V_{zl} given by

$$V_{\max} = 1 - \frac{1}{2\ln \rho}(V_\rho - 1 + \rho^2)\left[1 - \ln\left(\frac{V_\rho - 1 + \rho^2}{2\ln \rho}\right)\right]. \tag{28}$$

4.2. *Representation of input local flowrate ratio* R_{fl}

Substitution from eqn (24) into eqn (18) and then integration lead to

$$R_{fl} = \left[\sum_{i=1}^{L} \frac{b_i}{i+1}(r^{i+1} - \rho^{i+1})\right]\left[\sum_{i=1}^{L} \frac{b_i}{i+1}(1 - \rho^{i+1})\right]^{-1}, \tag{29}$$

for any given discrete velocity profile. Similarly, inserting the non-normalized form of eqn (27) into eqn (19) results in the local volume flowrate ratio for annular laminar flow

$$R_{fl} = \frac{1}{K_1}\left(\frac{r^2}{2}\left[1 + \frac{V_\rho - 1 + \rho^2}{\ln \rho}(\ln r - \tfrac{1}{2})\right] - \frac{r^4}{4} + K_2\right), \tag{30}$$

$$K_1 = \frac{1}{4}\left(1 - \frac{V_\rho - 1 + \rho^2}{\ln \rho}\right) + K_2, \tag{31}$$

$$K_2 = \frac{\rho^4}{4} - \frac{\rho^2}{2}\left[1 + \frac{V_\rho - 1 + \rho^2}{\ln \rho}(\ln \rho - \tfrac{1}{2})\right]. \tag{32}$$

As the desired inputs, V_{zl} and R_{fl} determined by eqns (25) and (29) or eqns (27) and (30) for either turbulent or laminar flow, respectively, act as average parameters to measure outputs V_{zp} and R_f of new point set f_p^M which is generated from f_p.

4.3. *Generation of new point sets*

The task of this section is to produce new point sets with desired kinetic or kinematic manners by using the known set f_p. The generating procedure of such a new set is said to be reliable for practical use provided that the following conditions are satisfied:

- The mass conservation principle holds under any circumstances; more specifically, the particle number of f_p cannot be altered when it is transformed to another one.
- The geometric configuration for a new point set can be either a circular or an annular domain so that the particle motion in a wide variety of jetflows can be simulated through the same mode.

The velocity or flowrate profile for a new point set is adaptive to changes in machining conditions and the accuracy is controllable.

Now attention is turned to constructing mathematical structures to realize the goal. A new point set f_p^M with velocity given by eqn (25) and flowrate ratio given by eqn (29) exists if it consists of points that are roots of L independent algebraic equations $R_{fl}(\zeta_k) = \bar{R}_f(r_k)$, $k = 1,2,...,L$, derived from eqns (25) and (29) or

$$\left[\sum_{i=1}^{L} \frac{b_i}{i+1}\left(\zeta_k^{i+1} - \rho^{i+1}\right)\right]\left[\sum_{i=1}^{L} \frac{b_i}{i+1}(1-\rho^{i+1})\right]^{-1} = 1 - (1-r_k)^{11/10}(1 + \tfrac{11}{10}r_k), \tag{33}$$

$$0 \le \rho \le \zeta_k \le 1,\ 0 \le r_k \le 1,\ \text{for } k = 1,2,...,L, \tag{34}$$

where $r_k = \sqrt{x_k^2 + y_k^2}$ is the radius of the kth point in f_p. The proof of this statement is not given here for sake of brevity. For a given r_k, one and only one real root ζ_k of eqn (33) should be found and taken as the radial coordinate of a point in f_p^M. The other coordinate of the point, the polar angle, is the same as that of the point (x_n, y_n) in f_p because the conversion is axisymmetric. After L roots are determined from eqn (33), the new point set formed is

$$f_p^M = \{(\zeta_1,\theta_1),(\zeta_2,\theta_2),...,(\zeta_L,\theta_L)\}, \tag{35}$$

$$0 \le \rho \le \zeta_i \le 1,\ 0 \le \theta_i = \arctan(y_i/x_i) \le 2\pi. \tag{36}$$

As demonstrated in Section 2, the values of r_k on the right-hand side of the equation vary unpredictably with the appearance order of the points. Additionally, b_i and ρ are also variables with respect to different velocity profiles and boundary conditions. Therefore, it is very difficult to confirm the existence and uniqueness of a root corresponding to a random r_k. Under such circumstances, in addition to a robust algorithm to produce f_p^M, the feedback process is indispensable. One of the key control variables is the error criterion for the accuracy of ζ_k because it has a crucial influence on the one-to-one transformation from f_p to f_p^M.

In a similar way, if annular laminar particle laden flow is described by eqns (27) and (30), the equation $R_{fl}(\zeta_k) = \bar{R}_f(r_k)$, for $k = 1,2,...,L$, for production of the new point set has the form

$$\frac{1}{K_1}\left(\frac{\zeta_k^2}{2}\left[1 + \frac{V_\rho - 1 + \rho^2}{\ln\rho}(\ln\zeta_k - \tfrac{1}{2})\right] - \frac{\zeta^4{}_k}{4} + K_2\right) = 1 - (1-r_k)^{11/10}(1 + \tfrac{11}{10}r_k). \tag{37}$$

This is a hypergeometric equation and its roots ζ_k cannot be expressed explicitly.

4.4. *Feedback verification*

After the formation of a new functional point set f_p^M, the main concern of practical interest is to check its correctness and accuracy. In doing so, the feedback parameters are V_{zp} and R_f and they are calculated by $R_f = N_{xy}/N_0$ and $V_{zp} = [R_f(\zeta_i) - R_f(\zeta_{i-1})]/[\zeta_i(\zeta_i - \zeta_{i-1}]$ based on eqns (18) and (22). Consequently, the desired inputs V_{zl} and R_{fl} actually serve as the average measurement of V_{zp} and R_f. The results show that V_{zp} and R_f of f_p^M might greatly deviate from the desired inputs if the roots of eqn (33) or eqn (37) are out of the controllable limitations.

It is important to point out that the desired input variables are not always time-independent but alter with machining conditions. For example, during deep drilling, the backflow within the hole will dramatically shape the velocity profile of jetflow. In such circumstances, when the signals of a sensor, such as acoustic signals in the on-line control

process, feed back the depth value of a hole, the input velocity profile should be simultaneously adapted to a suitable status.

Four patterns are given in Fig. 5 to illustrate the effectiveness of the control process. Note that R_{fl} and R_f are accurately consistent with each other. Despite its oscillating feature, V_{zp} fluctuates around the average value V_{zl}. Calculations show that in the vicinity of points $dR_f/dr = 0$ and/or $dV_{zp}/dr >= 0$, the accuracy of numerical data for V_z is very sensitive to the increment $\Delta r = r_i - r_{i-1}$ and initial value r_0 of radius r. This is the main reason why curves of V_z oscillate manifestly around these points. Once f_p^M is confirmed as being capable of performing the kinematic function, its velocity profile is replaced by V_{zl} in the machining simulation so that the oscillating feature will not significantly influence the accuracy of the final results. Note that the particle distribution is the function of radius and it is controlled by R_j.

The oscillating characteristic of V_{zp} mainly results from the replacement of three-phase continuum flow by discrete particle flow. As a matter of fact, with the increase of the particle number, the oscillation alleviates significantly.

5. SIMULATION AND VERIFICATION

5.1. *Simulation*

New point sets obtained from the feedback control process can be utilized to calculate erosion rates of solid materials. Theoretically speaking, the simulation of a machining operation by AWJ is to trace trajectories of particles and to evaluate individually their penetrating ability during the movement of jetflow along the nozzle. The availability of point sets with desired velocity profiles and local flowrates realizes this idea.

To record histories of particles, the workpiece surface to be cut is divided into a network of finite elements and each element of this network acts as a memory cell which stores kinetic information of particles, as shown in Fig. 6. Being the particle source, f_p^M spreads its points (particles) over the cutting region when it goes forward with the nozzle. The kinetic energy E_k stored within the ith cell is given by

$$E_k(X_i, Y_i) = \tfrac{1}{2} m \sum_{j=1}^{s_i} [V_j(t_j, X_i, Y_i)]^2, \tag{38}$$

where m is the average mass of particles, s_i is the sum of particles stored in the ith cell, $V_j(t_j, X_i, Y_i)$ is the velocity of the particle which falls into the cell at instant t_j, and (X_i, Y_i) are the coordinates of the geometrical center of the cell. A particle moving through the nozzle will be trapped by the ith cell if it invades the area covering the size of the cell.

Many sophisticated analyses consistently show that the volume Ω removed by a particle from the workpiece is directly proportional to its velocity, i.e. $\Omega \propto V^\lambda$, where λ is a physical constant [5–9]. If the cell-to-cell interaction and the depth–velocity coupling effect are ignored, after certain calculations the maximum depth $H(X_i, Y_i)$ of cut for the ith cell can be expressed by

$$H(X_i, Y_i) = \sum_{j=1}^{s_i} g_j(t_j, X_i, Y_i)[V_j(t_j, X_i, Y_i)]^\lambda, \tag{39}$$

where $g_j(t_j, X_i, Y_i)$ is a synthetic function relevant to the AWJ machining parameters and to material properties of the workpiece and particles. For the shallow cutting, $H(X_i, Y_i) \leq$ 20 mm, for example, the $g_j(t_j, X_i, Y_i)$ can be taken as a constant which is determined by experiments. A three-dimensional cut kerf is the combination of many depths for different

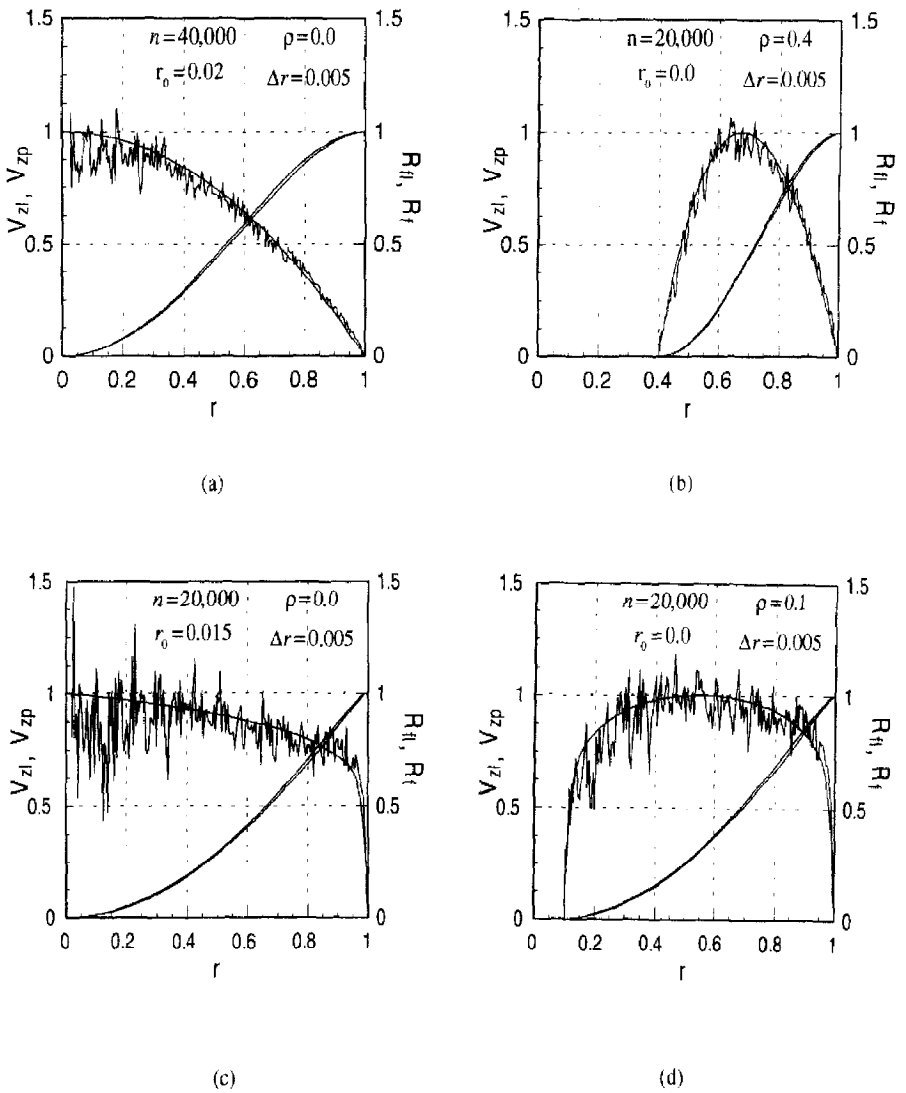

Fig. 5. Comparison between desired input (V_{zl}, R_{fl}) and output (V_{zp}, R_f): (a) conventional laminar flow; (b) annular laminar flow; (c) conventional turbulent flow from $V_{zl} = (1-r)^{1/7}$; (d) annular turbulent flow simulated by $V_{zl} = (1-r)^{1/5}(r-0.1)^{1/5}$.

cells in the erosion area. In the present research, the seventh power law of turbulent pipe flow is used as the velocity profile of particle-laden jetflow [4].

As discussed previously, experiments demonstrate that the surface quality resulting from AWJ machining is relevant to the chaotic behavior of particles. To confirm this by the present model, two patterns for one-pass cut are plotted in Fig. 7, where the z coordinate stands for the dimensionless depth of cut.

One can see from Fig. 7 that when the traverse speed of the nozzle increases from 0.5 mm/s to 3.0 mm/s the waviness and roughness of lateral surfaces and bottom become very significant for the same depth of cut. Analytical results are consistent with many well-known experiments. The extremely irregular features can be contributed to the disordered motion of particles. In fact, faster movement of the nozzle leads to fewer particle

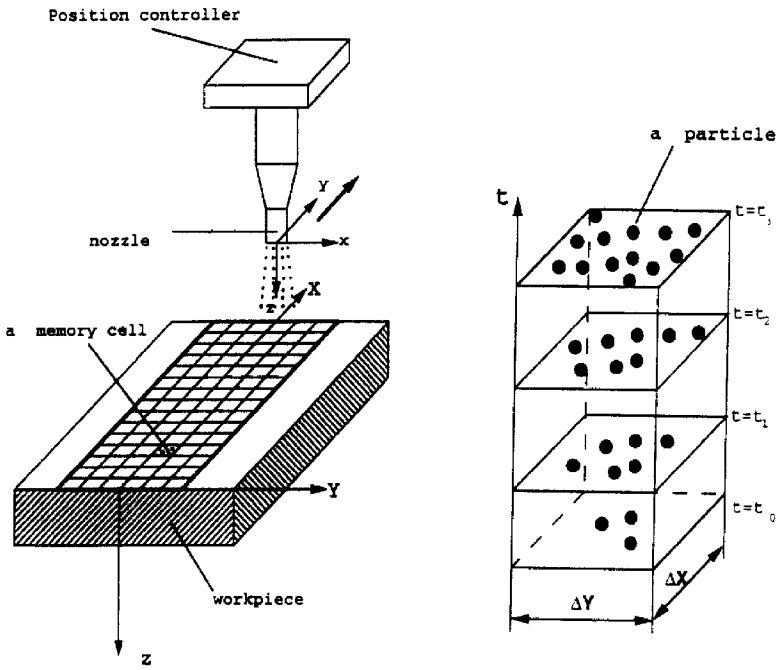

Fig. 6. Illustration of the machining simulation process with the memory cell network.

impacts and therefore irregular particle motion becomes more obvious over the entire region.

It is interesting to point out that the present model is the only model to date which is capable of illustrating underlying mechanisms of surface characteristics appearing in the experiments. The advantage is attributed to the application of chaotic point sets to the machining simulation.

5.2. *Experiment*

Two groups of experimental data are achieved through cutting titanium and aluminum. One includes the macro machining parameter-depth of cut, the other shows the micro machining parameters-waviness of lateral surface. For the depth of cut, a measurement is taken three times along a path of partial penetration, and the average value is listed in Table 1. The waviness of lateral surface is defined as the difference between the peak value and the valley value of irregularity on the surface, as shown in Fig. 8. Because of the small scale, the results in Table 2 are achieved with the aid of the microscope. The comparison between theory and experiment shows that simulation has a satisfactory accuracy for both macro and micro parameters despite the certain error variation for waviness due to the complexity of surface irregularities.

6. CONCLUSION AND DISCUSSION

Theoretical and experimental results show that acting as a particle source in three-phase axisymmetrical jetflow, a point set with chaotic and kinetic features can be used to simulate abrasive waterjet machining. This research mainly consists of three parts. First, a new Julia

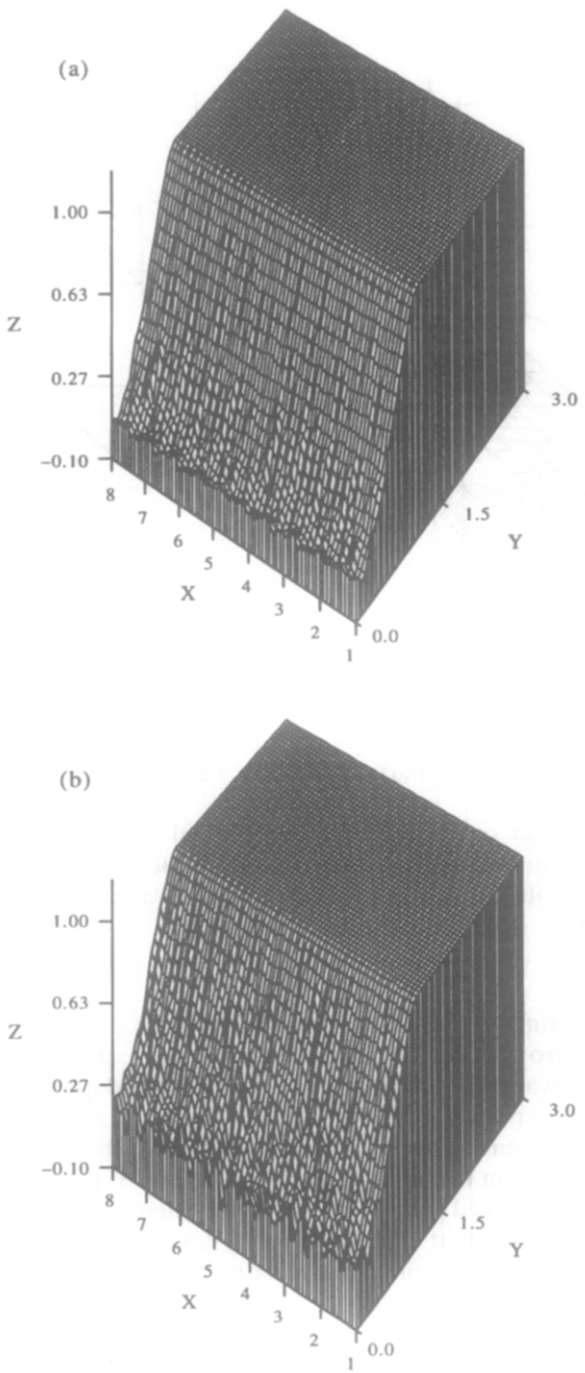

Fig. 7. The cutting view of a partial penetration from simulation results with the abrasive flowrate $\dot{m} = 12 \times 10^4$ particles/s and traverse rate of the nozzle (a) $u_x = 0.5$ mm/s; (b) $u_x = 3.0$ mm/s.

Table 1. Experimental and theoretical results for depth of partial penetration from cutting titanium, where u_z is the traverse rate of the nozzle, and h_e the experimental value of depth of cut

u_z [mm/s]	8.0	7.0	6.0	5.0	4.0	3.0	2.0
h_e [mm]	4.7	5.6	7.0	8.3	11.0	15.1	18.2
h_t [mm]	5.3	6.0	7.0	8.4	10.5	14.0	20.8

Workpiece material: titanium; abrasive material: aluminum oxide; size of abrasives: 100 (mesh); diameter of mixing tube: 1.54 mm; waterjet pressure: 300 mpa; abrasive flowrate: 5.4 g/s; standoff distance: 12.7 mm.

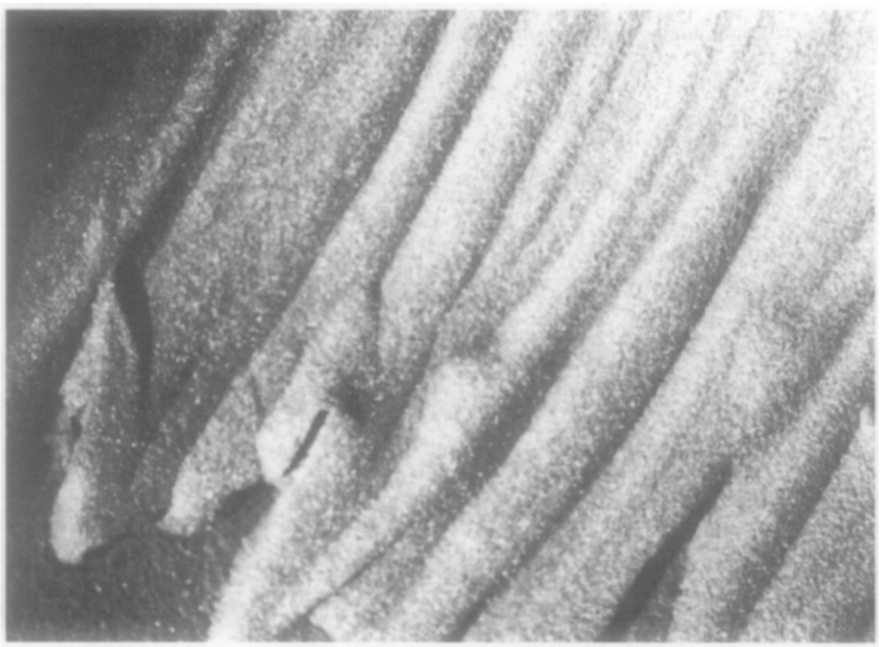

Fig. 8. Micro view (× 125) of waviness on the lateral surface of a partial penetration.

set is discovered and it proves to possess chaotic and axisymmetric characteristics which match with the nature of particle motion on the annular or circular cross-section of particle-laden flow. Secondly, combined with the new point set, a robust feedback control process is designed to produce new particle sources for describing general particle motion with any desired velocity profiles and local flowrates. And thirdly, the particle motion

Table 2. Experimental and theoretical results for waviness of the lateral surface of partial penetration from cutting aluminum, where u_z is the traverse rate of the nozzle, $z = h_t/(h_t)_{max}$ is the dimensionless depth of cut and w is the waviness [mm]

u_z [mm/s]		1.0	2.0	3.0	4.0
$z = 0.2$	w_t	0.000	0.021	0.028	0.035
	w_e	0.020	0.029	0.020	0.032
$z = 0.4$	w_t	0.021	0.043	0.043	0.064
	w_e	0.050	0.040	0.046	0.064

Waterjet pressure: 250 mPa; abrasive material: garnet (100 mesh); diameter of mixing tube: 0.8 mm; abrasive flowrate: 2.57 g/s; standoff distance: 6 mm; workpiece material: aluminum.

simulation is successfully applied to characterize the surface quality of the cutting surfaces and estimate the erosion rate of abrasive particles. Results show that chaotic features of particle motion have crucial influences on the waviness and roughness of surfaces.

Simulation and control of particle motion in pipe flow is just in its primary stage. Many topics are open to further research, such as simulation and control of particle motion in non-axisymmetric pipe flow with non-steady features. In addition, it is also an intriguing topic to find the coherent relation between simulation results and governing equations of fluid mechanics.

Acknowledgement—The authors would like to thank the National Science Foundation for the support of this project under Grant DMI-9523010.

REFERENCES

1. Yong, Z. and Kovacevic, R., Fundamentals of constructing particle-laden flow by fractal point sets and predicting 3D solid erosion rates. *Chaos, Solitons & Fractals*, 1997, **8**, 207–220.
2. Shinbrot, T., Grebogi, C., Ott, E. & York, J. A., Using small perturbations to control chaos. *Nature*, 1993, **363**, 411–417.
3. Ott, E. & Spano, M., Controlling chaos. *Physics Today*, 1995, **May**, 34–38.
4. Shames, I. H., *Mechanics of Fluids*. McGraw–Hill, New York, 1962.
5. Bitter, J. G. A., A study of erosion phenomena, Part I. *Wear*, 1963, **16**, 5.
6. Finnie, I., The mechanisms of erosion of ductile metal. In *Proceedings of the Third National Congress of Applied Mechanics*, ASME, 1958, pp. 527–532.
7. Gulden, M. E., Solid particle erosion of high technology ceramics. *ASTM STP664*, ed. W. F. Adler, 1979, pp. 101–122.
8. Hashish, M., A modeling study of metal cutting with abrasive-waterjets. *ASME J. Engng Materials Technol.*, 1984, **106**, 88–100.
9. Yong, Z. and Kovacevic, R., Simulation of effects of water-mixture film on impact contact in abrasive waterjet machining. *Int. J. Mech. Sci.*, 1997 (in press).